APPLIED SCIENCES AND ENGINEERING

The size effect in corrosion greatly influences the predicted life span of concrete infrastructures

Ueli M. Angst[1]* and Bernhard Elsener[1,2]

Forecasting the life of concrete infrastructures in corrosive environments presents a long-standing and socially relevant challenge in science and engineering. Chloride-induced corrosion of reinforcing steel in concrete is the main cause for premature degradation of concrete infrastructures worldwide. Since the middle of the past century, this challenge has been tackled by using a conceptual approach relying on a threshold chloride concentration for corrosion initiation (C_{crit}). All state-of-the-art models for forecasting chloride-induced steel corrosion in concrete are based on this concept. We present an experiment that shows that C_{crit} depends strongly on the exposed steel surface area. The smaller the tested specimen is, the higher and the more variable C_{crit} becomes. This size effect in the ability of reinforced concrete to withstand corrosion can be explained by the local conditions at the steel-concrete interface, which exhibit pronounced spatial variability. The size effect has major implications for the future use of the common concept of C_{crit}. It questions the applicability of laboratory results to engineering structures and the reproducibility of typically small-scale laboratory testing. Finally, we show that the weakest link theory is suitable to transform C_{crit} from small to large dimensions, which lays the basis for taking the size effect into account in the science and engineering of forecasting the durability of infrastructures.

INTRODUCTION

Chloride-induced corrosion of reinforcing steel in concrete, for decades, has been one of the largest challenges worldwide in maintaining the condition of civil engineering structures and thus ensuring reliability, safety, and sustainability of these infrastructures (*1*–*5*). Over the coming decades, the situation can be expected to be aggravated (*6*), owing to the continuous aging of the infrastructure, the large majority of which was in industrialized countries built in the middle of the past century. However, there is still a lack of fundamental understanding about what controls corrosion initiation in concrete.

Concrete structures are exposed to chlorides not only in marine environments but also in the many regions of the world where deicing salts are used on roads as a means to improve traffic safety during the winter season. Being a porous material, concrete permits penetration of chloride ions through the liquid phase contained in the pore system. Once a sufficiently high chloride concentration is reached at the reinforcing steel surface, initiation of localized corrosion is possible. This type of corrosion attack is particularly dangerous because it is associated with the formation of macrocells, wherein relatively small anodic sites are galvanically coupled with relatively large cathodic areas (*4*, *7*), thereby giving rise to high local rates of steel cross-sectional loss. The local rate of cross-sectional loss may reach values of 0.1 to 1 mm/year under some conditions (*4*), which can severely impair the serviceability or load-bearing capacity of a structure within a relatively short time.

Awareness of degradation of concrete structures owing to chloride-induced corrosion gained momentum during the second half of the past century. Over the following decades, an engineering approach was established using a concept similar to traditional structural mechanics, wherein failure may be described by comparing the mechanical load to the material strength (that is, ultimate limit state design). In durability engineering, the load analogously corresponds to the concentration of chlorides reached at the steel surface in the concrete, whereas the material strength is understood as a chloride threshold concentration for the occurrence of corrosion.

On the basis of this conceptual approach to predicting corrosion initiation, a vast amount of research has been aimed at modeling chloride penetration through concrete (*8*)—as a function of exposure conditions, concrete properties, etc. On the other hand, a substantial amount of research was devoted to determining the chloride threshold level for corrosion initiation, the so-called critical chloride content in the concrete (C_{crit}). Because C_{crit} directly describes the limit state (that is, the transition from a noncorroding to a corroding structure), this parameter is of uttermost importance in service life design or predictions and in the condition assessment of existing structures. From today's perspective, we can conclude that particularly the search for C_{crit} has turned out as a difficult endeavor. In this regard, a number of reviews of the extensive body of literature have consistently revealed that C_{crit} scatters over a large range, both for laboratory results and for data collected from engineering structures (*9*–*11*). This may, at least partly, be explained by different conditions at the surface of reinforcing steel in concrete that are expected to play a role in corrosion initiation (*12*).

A detailed review by Angst *et al.* (*13*) of the steel-concrete interface (SCI) revealed pronounced spatial variability in terms of chemical and physical properties at the surface of steel embedded in concrete. Considering that the length scale along the steel surface of some of these local characteristics is on the order of centimeters, it can be expected that the probability for the absence or presence of certain features is significantly influenced by the exposed steel surface area, particularly for specimen dimensions typically used in laboratory studies. Consequently, an influence of the specimen size on C_{crit} can be expected.

In pursuit of elucidating the role of different characteristics at the SCI in corrosion initiation in concrete, we examined the location of corrosion initiation in laboratory-manufactured reinforced concrete specimens with respect to characterization of various features at the SCI, primarily examining steel metallurgy and voids in the concrete. Our results from testing specimens of different lengths (Fig. 1A) confirm the hypothesis that the size of the exposed steel surface has an influence on C_{crit}. As will be discussed, this size effect strongly

[1]Institute for Building Materials, ETH Zürich, Stefano-Franscini-Platz 3, Zurich CH-8093, Switzerland. [2]Department of Chemical and Geological Science, University of Cagliari, I-09100 Monserrato, Cagliari, Italy.
*Corresponding author. Email: uangst@ethz.ch

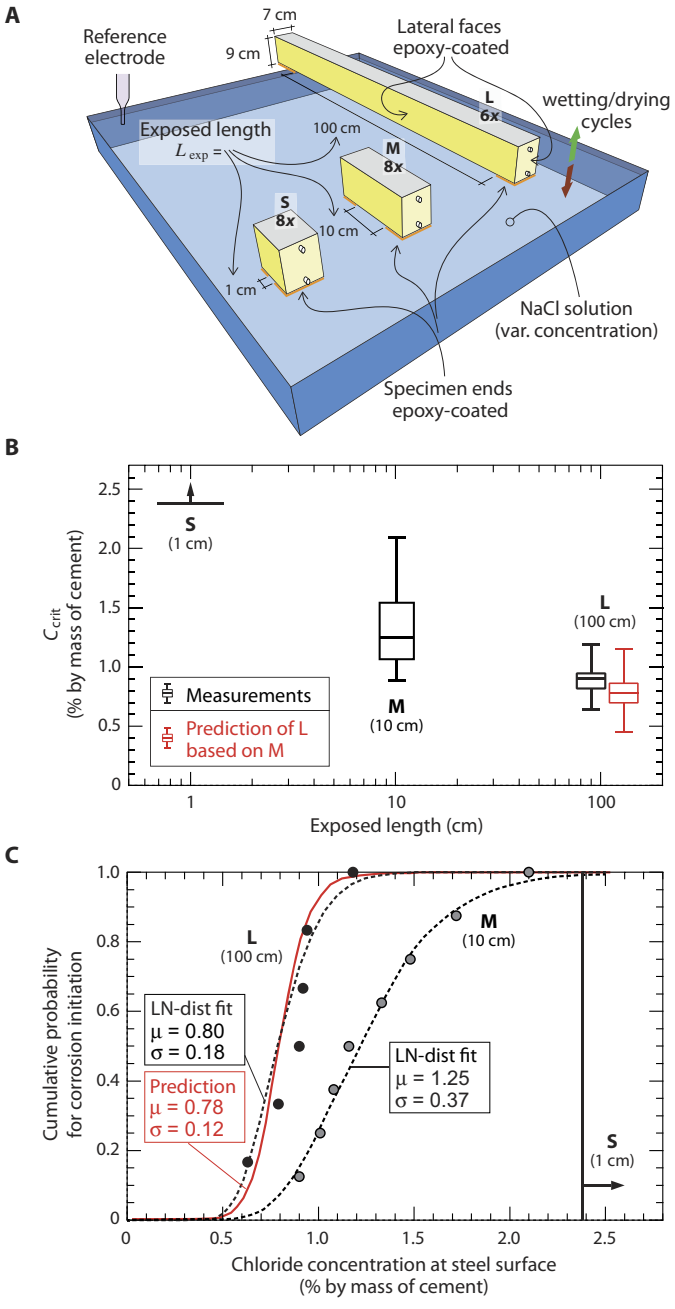

Fig. 1. Effect of specimen size on the chloride concentration needed for corrosion initiation of carbon steel in concrete. (**A**) Setup for corrosion tests of reinforced concrete specimens under chloride exposure with three different exposed lengths, labeled L (100 cm), M (10 cm), and S (1 cm). The number of tested specimens is also indicated. (**B**) Box plots of measured C_{crit} (black) shown for the different L_{exp} (whiskers, min/max; red box plot, prediction for size L) based on the probabilistic model and on the results for M (compare discussion section for details). (**C**) Cumulative probability for corrosion initiation as a function of the chloride concentration. Dots represent individual measurements, the dashed lines are fits assuming a log-normal distribution, and the red line is the prediction based on the probabilistic model. μ and σ are the first two moments of the log-normal distributions. The smallest specimens (L_{exp} = 1-cm exposed length) did not corrode even at a chloride concentration of 2.38%.

affects the established conceptual approach of forecasting corrosion in concrete.

RESULTS

The specimen size influences susceptibility to corrosion

The chloride concentration at the steel surface needed to initiate corrosion decreases with increasing length of the reinforced concrete beams exposed to chlorides (Fig. 1 and table S1). Small laboratory specimens tolerate higher chloride concentrations than larger specimens. For specimens with 10-cm exposed reinforcing steel length (L_{exp} = 10 cm), the observed chloride threshold values for corrosion range from 0.9 to 2.1% chloride by mass of cement, whereas for 100-cm-long reinforcing steel bars, chloride concentrations of 0.6 to 1.2% by mass of cement were sufficient to initiate corrosion. In the smallest specimens studied in this work (L_{exp} = 1 cm), no corrosion was observed during the test period. The corresponding chloride concentration at the steel depth in these noncorroding specimens was determined at 2.4% by mass of cement (table S1). This may be considered as a lower limit of C_{crit} of the specimens with an exposed length of 1 cm.

In addition, Fig. 1 shows that increasing specimen size diminishes the scatter in the obtained results. The SD in chloride threshold value for L_{exp} = 100 cm was roughly half of the SD of specimens with L_{exp} = 10 cm.

Corrosion does not preferentially initiate at coarse voids

After corrosion initiation had been detected by means of electrochemical, nondestructive measurements, the location of pitting corrosion initiation was assessed by visually inspecting the SCI upon splitting the concrete specimen and removing the reinforcing steel bar from the concrete (Fig. 2A). The sites where localized corrosion had initiated were clearly visible because typically black corrosion products were deposited on the steel and the adjacent concrete. Often, the initially dark spots were surrounded by red/brown corrosion products deposited up to several centimeters away from the initiation site. In addition, the dark corrosion products gradually turned red/brown upon exposure to air. This was interpreted as oxidation of those corrosion products that had, under deoxygenated conditions, been deposited at the anodic site, which is typical for the process of localized (pitting) corrosion, wherein anodic and cathodic sites are spatially separated and macrocells are formed (*4*).

Visual inspection revealed the inhomogeneous nature of the SCI. In particular, voids covering a wide range of spatial dimensions were frequently found (Fig. 2, A and B, and fig. S1). These include air voids resulting from air bubbles in the fresh concrete that become trapped at the steel surface (*14*, *15*). Although some of the visually apparent entrapped air voids were small (diameter of approximately 0.1 mm), others reached dimensions of up to 10 mm. The spacing between these voids at the steel surface ranged from a few millimeters to a few centimeters; several entrapped air voids were found within the exposed rebar portion in each of the investigated concrete specimens, including coarse voids with diameters of several millimeters.

Nevertheless, corrosion never coincided with the location of coarse voids (that is, voids larger than approximately 1 mm in diameter). For smaller voids, it was difficult to draw conclusions due to the masking effect of precipitated corrosion products.

Figure 2 (C and D) shows the pronounced change in conditions at the steel surface in the presence of an air void. There is a marked transition between different zones, namely, steel in contact with bulk

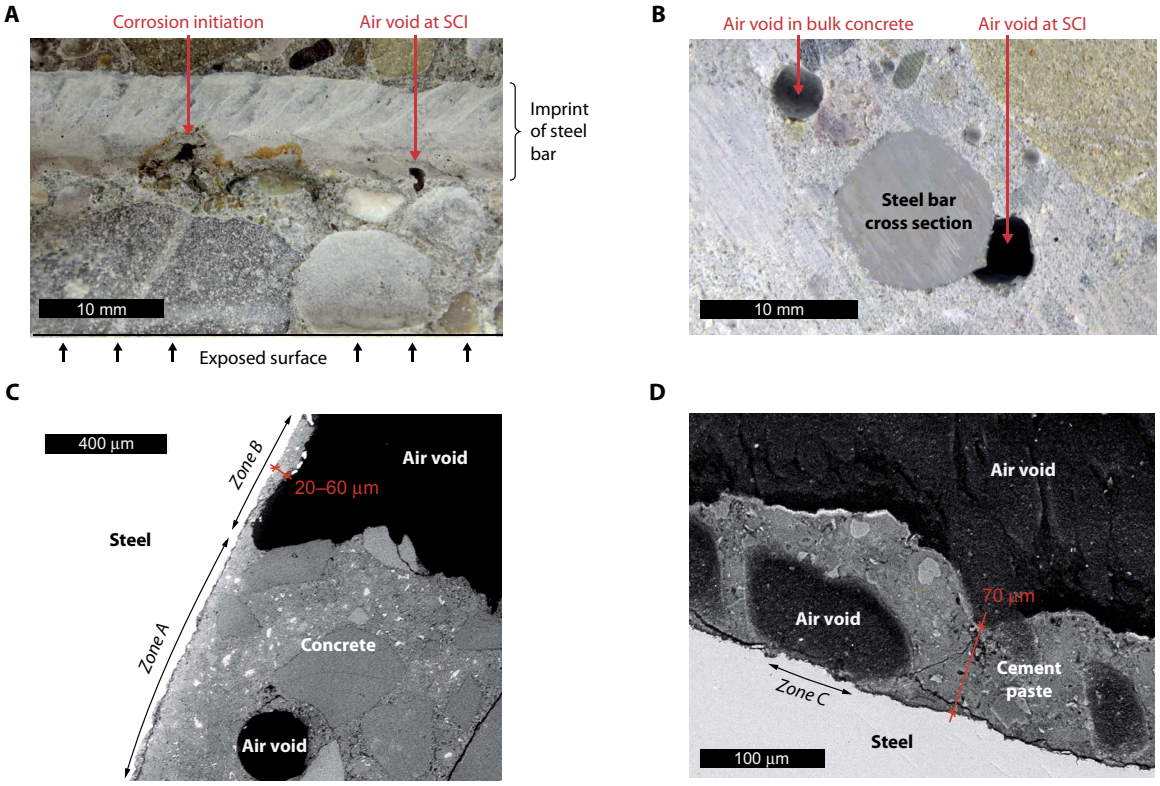

Fig. 2. Inhomogeneities at the SCI. (**A**) Representative image of a split concrete specimen after removal of the steel bar, showing dark corrosion products at the location of corrosion initiation, surrounded by a rim of red/brown deposited rust and the presence of a coarse air void at the steel surface (free from corrosion). (**B**) Image of a section perpendicular through the steel bar in concrete with a coarse air void at the SCI. (**C**) Backscattered electron (BSE) micrograph of a polished section perpendicular to the steel bar of an epoxy-impregnated specimen illustrating the transition of the SCI morphology from zone A (steel in contact with concrete) to zone B (at coarse air void, where the steel is covered with a thin layer of cement paste). (**D**) SEM micrograph of a carbon-coated section perpendicular to the steel bar showing the presence of a cement-paste layer on the steel surface that is interspersed with small air voids.

concrete (zone A) and steel covered with thin layer of cement paste, which is exposed to air in the air void (zone B). In this example, the thickness of the cement paste layer was 20 to 60 µm, but other cases with slightly thicker layers (70 to 120 µm) were also observed, which may contain smaller air voids themselves (Fig. 2D). Within these pores, it appears that the steel surface has almost no cementitious covering, that is, that virtually bare steel is exposed to the air in the void (zone C).

Initiation sites correspond to metallurgical features

Inspection of the reinforcing steel bars that had been removed from the concrete upon corrosion initiation typically revealed the presence of one distinct corroding spot, which in some cases was surrounded by significantly smaller corrosion pits, all of them within an area of maximum approximately 5 mm^2 (fig. S2). The small corrosion pits were interpreted as sites where corrosion had initiated but was not able to reach stable pit growth (in contrast to the dominating corrosion site) (*16*). However, several pronounced areas of localized corrosion close to each other were occasionally observed within a steel surface area of <1 cm^2 (Fig. 3A). Visual examination also revealed that in 75% of all cases, corrosion initiated between the rebar ribs or directly at the rib edge (Fig. 3A and fig. S2).

Analyses of cross sections of steel bars indicated that the morphology of the corrosion attack resembled shallow or cone-shaped corrosion pits (Fig. 3B and fig. S2). These pits were typically covered with a crust of corrosion products, which occasionally remained even after the chemical cleaning process in inhibited hydrochloric acid. In some cases, at the bottom of the corrosion pit, relatively deep branches of corrosion attack were found to extend into the steel (Fig. 3C). Corrosion appeared to penetrate preferentially along grain boundaries and by dissolving the pearlite phase of the steel microstructure. Finally, Mn-Si oxide inclusions were found to be strongly inhomogeneously distributed across the steel cross section, and corrosion initiated preferentially—but not exclusively—at those areas of the steel bar where the Mn-Si oxide inclusions reached the surface.

The ferritic-pearlitic microstructure shown in Fig. 3C was found homogeneously across the entire steel bar cross section. This is characteristic for cold-deformed reinforcing steel bars as the ones used in this study. Because of the manufacturing process, cold-deformed reinforcing steel bars are typically free from mill scale, which was confirmed in all analyzed metallographic samples. None or only very small remnants of mill scale or native corrosion products were found on the reinforcing bar surface.

DISCUSSION

The size effect is caused by inhomogeneities along the steel surface

Our findings show that the chloride concentration needed to initiate corrosion of reinforcing steel in concrete significantly depends on the size of the investigated specimens. We suggest that this size effect can

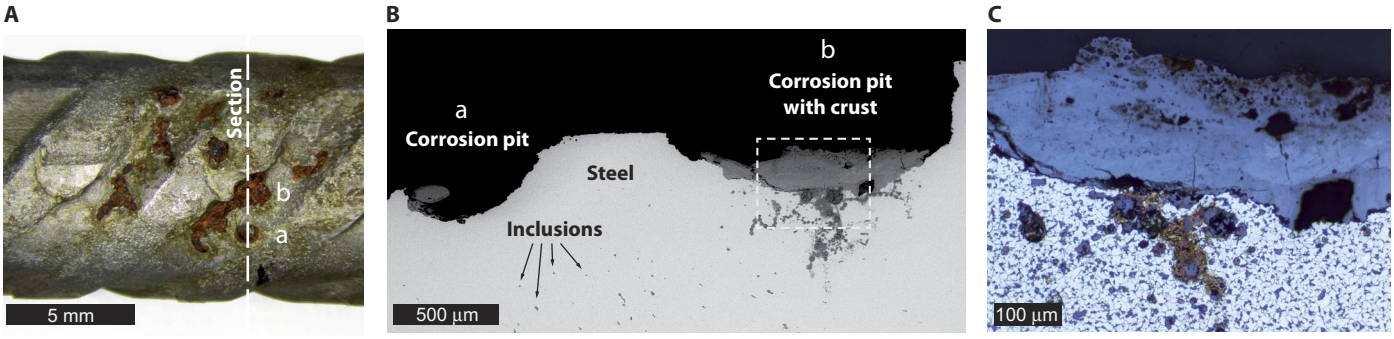

Fig. 3. Corrosion morphology. (**A**) Close-up image of a steel bar after removal from the concrete and after chemical cleaning showing several sites of localized corrosion within an area of <1 cm^2. (**B**) BSE micrograph of the section indicated in (A) showing two shallow corrosion pits, a and b. Pit b is covered with a crust of chloride containing iron complexes, underneath which branched corrosion attack extends into the steel. The dark spots in the steel are inclusions (MnO, SiO_2, and FeO). (**C**) Light optical micrograph of the etched section of the framed portion of (B) showing the ferritic-pearlitic microstructure and the preferential corrosion attack of the pearlite phase of the Mn-Si oxide inclusions and along grain boundaries.

be explained by inhomogeneities at the steel surface, namely, by the spatial variability of physical and chemical conditions of the SCI, which is influenced by properties of both the reinforcing steel and of the concrete. Increasing the specimen size will thus increase the probability for the presence of conditions favoring corrosion initiation at lower chloride concentrations. These may include zones of particularly corrosion-susceptible steel metallurgy (for example, accumulations of inclusions) or areas where the concrete adjacent to the steel offers low corrosion protection.

From experiments of localized corrosion on passive metals, such as stainless steel in aqueous solutions, it is well known that initiation of pitting corrosion is governed by local features (*17*). Depending on the presence or absence of certain preferential initiation sites within the tested surface area, the susceptibility of a sample surface to pitting corrosion will be higher or lower, respectively. This was experimentally confirmed by measurements of pitting potentials of passive steels in aqueous chloride solutions (*18*, *19*) and already recognized early by Evans (*20*), who pointed out that the reproducibility of experiments with small specimens to study localized corrosion phenomena can be poor. In corrosion studies in solutions, all inhomogeneities can be reasonably assumed to be related to the metal, rather than to the exposure environment.

However, for steel in concrete, further spatial variability is introduced because of the inhomogeneous nature of the composite material concrete. As recently summarized by Angst *et al.* (*13*), the SCI in engineering structures may exhibit significant variability in terms of local properties, arising from the local presence or absence of concrete cracks, honeycombs, voids of different origin, spacers, tie wires, mill scale, native rust layers, steel surface contaminants, etc. Several of these characteristics are generally believed to play a role in corrosion initiation, for example, air voids (*21*), bleed-water zones (*22*, *23*), or crevices in the mill scale (*24*). They may thus act as "weak spots" (that is, areas particularly susceptible to corrosion along the steel surface).

In the present laboratory study, the SCI was free from most of these features expected for engineering structures. The main inhomogeneities in this work were concrete voids at the SCI and metallurgical variability (for example, inclusions). Although our findings suggest that coarse entrapped air voids at the SCI are not preferential sites for corrosion initiation, metallurgical features and aspects related to the steel bar geometry (ribs) seem to favor corrosion initiation.

The observation that coarse air voids were harmless under the present wetting/drying exposure conditions can be explained by the fact that they were not filled with solution. Even for continuously submerged concrete, an air void diameter of >0.5 mm likely needs several years, or even decades, to become water-saturated (*13*, *25*, *26*). However, smaller air voids, such as those on the order of a few tens of micrometers in size (Fig. 2D), may have reached saturation within the exposure time in this study of up to 1.5 years. Although a possible correlation of these small air voids and of corrosion initiation sites could not be investigated, owing to the masking effect of deposited corrosion products, it cannot be excluded that small air voids may have contributed to corrosion initiation in this study. The observation that coarse air voids (that is, air voids visible to the naked eye) under cyclic wetting/drying exposure are not preferential sites for corrosion initiation, even with prolonged wetting periods of several months, is in agreement with other recent experimental results (*27*, *28*). On the other hand, for water-saturated concrete, corrosion initiation was reported in the literature to be facilitated by the presence of coarse air voids at the SCI (*21*).

It was also observed that most of the corrosion initiation sites were located between the ribs of the reinforcing steel bars (Fig. 3A). Although this may be attributed to metallurgical weaknesses (for example, lattice dislocations caused by cold work hardening and deforming of the reinforcing bars during manufacturing), it may also be due to different concrete properties in these areas. The reinforcing steel bars were oriented vertically during concrete casting. Horne *et al.* (*29*) have shown that for vertical reinforcing steel bars, the concrete porosity is higher underneath ribs compared to bulk concrete and that gaps may form at these undersides due to the accumulation of bleed water. As a result, portlandite—the presence of which at the steel surface in concrete has early been suggested to be one of the main corrosion protective actions of concrete for the embedded steel (*1*)—is locally lacking in bleed-water zones. This may explain why corrosion preferentially initiated at locations between ribs.

Finally, in addition, penetration of chlorides through the concrete cover is likely inhomogeneous, giving rise to spatial variability of the chloride concentration at the steel surface (*30*–*33*). In summary, the probability for a sufficiently high chloride concentration at the steel surface, matching a sufficiently low resistance to chloride-induced corrosion owing to the discussed local characteristics at the SCI, increases with specimen size. In engineering structures, the SCI is presumably more inhomogeneous compared to the SCI of the laboratory specimens in the present work (*13*). As a result, the size effect may be even more pronounced.

C_{crit} and the weakest link theory

As discussed in the previous section, corrosion always initiates first at the weakest spot of the exposed steel surface area (that is, at the spot most susceptible to corrosion). Large specimens can be regarded as a combination of small specimens. In the present case, for instance, one L-type specimen (L_{exp} = 100 cm) would correspond to a combination of 10 M-type specimens (L_{exp} = 10 cm). In this hypothetical L-type specimen, the chloride concentration at which corrosion would initiate corresponds to the minimum C_{crit} of the 10 M-type specimens. Following this reasoning, the weakest link theory (*34*) may permit predicting the distribution of C_{crit} for various L_{exp}, given the distribution of C_{crit} for small-scale laboratory specimens (*35*). To predict the C_{crit} of L-type specimens based on the experimental results from the M-type specimens, the following equation applies (*35*)

$$p_L = 1 - (1 - p_M)^k \quad (1)$$

Here, p_L and p_M are the probabilities for corrosion for series L and M, respectively [that is, $p = P(C_{crit} \leq$ chloride content)], and k is the ratio of L_{exp} of the two series (that is, k = 10). The red box plot in Fig. 1B and the red line in Fig. 1C show the result (that is, the prediction of C_{crit} at L_{exp} = 100 cm) using Eq. 1 and the log-normal distribution at L_{exp} = 10 cm as input data. This prediction is in agreement with the experimental results obtained for L_{exp} = 100 cm.

Thus, the approach presented here appears to be suitable to transform C_{crit} values that were determined for a certain specimen size to another, larger specimen size. Ultimately, application of the weakest link theory to chloride-induced corrosion in concrete may significantly contribute to successful translation of laboratory results to engineering structures.

Size effect compared to other influencing factors

Parameters that are generally considered important for the durability of reinforced concrete are the type of cement (binder) and the water/binder ratio (w/b) in the concrete (*4*, *5*). A number of authors studied the influence of w/b and binder on C_{crit}, but there is no general quantitative agreement. This can be related primarily to differences in experimental conditions and measurement techniques used in different studies (*11*).

Nevertheless, lowering the w/b ratio was generally found to increase C_{crit} (*36*–*40*). On the basis of these literature results, a decrease of w/b from 0.6 to 0.4 can be estimated to increase C_{crit} by a factor of approximately 1.5 on average (varying in a range of approximately 1.2 to 2.1). Note that changing w/b from 0.6 to 0.4 is considered to significantly affect most concrete properties (*4*, *5*, *41*). Thus, although this range covers a substantial proportion of concretes used in practice, the impact on C_{crit} appears to be moderate.

With regard to the influence of cement type on C_{crit}, fly ash and blast furnace slag are the mineral admixtures that have been the most intensively studied (*11*). Nevertheless, literature is contradictory, meaning that both adverse (*39*, *42*, *43*) and beneficial (*44*), as well as negligible (*9*, *45*), effects on C_{crit} have been reported for these mineral admixtures. Concerning 30% fly ash replacement, for instance, Thomas (*43*) and Oh *et al.* (*39*) reported a decrease of C_{crit} by a factor of 0.7, whereas Schiessl and Breit (*44*) found an increase of C_{crit} by a factor of 1.6, and Alonso *et al.* (*45*) found no significant influence.

Our findings in Fig. 1 show that decreasing the specimen size from 100- to 10-cm rebar length increases the mean of C_{crit} by a factor of 1.44; decreasing the specimen size further has an even more pronounced effect on C_{crit}. Thus, the size effect seen in the range of typical laboratory-specimen dimensions and of practical structures (see next section) may be considered at least comparable to the influences cement type and w/b ratio. Nevertheless, it has to be noted that our results were obtained from a limited range of material properties (ordinary Portland cement, w/b = 0.5, cold-work strengthened reinforcing steel in "as-received condition," etc.) and that varying these material parameters may have an influence on the size effect, that is, that the size effect may be more or less pronounced for certain configurations of experimental parameters.

Implications for laboratory testing and for service life predictions

Given the relative importance of the specimen size with respect to other parameters generally considered important for the corrosion performance of reinforced concrete, we believe that the size of specimens (that is, the exposed steel surface area) needs to receive more attention in future research and in engineering. The length of the exposed steel bar in laboratory corrosion investigations usually ranges from 5 to 30 cm [for example, studies cited in Angst *et al.* (*11*)]. This corresponds to steel surface areas of ~10 to 80 cm^2, thus of much smaller dimensions than those of structural members in engineering structures. This has implications both for laboratory testing and for applying laboratory results to practice.

The fact that the variability in C_{crit} increases when smaller specimens are used (Fig. 1) affects the reliability of experiments. The smaller the specimen dimensions are, the poorer the reproducibility of an experiment becomes. Given a certain L_{exp}, this can only be counteracted by increasing the number of parallel specimens. By means of probabilistic considerations, Angst *et al.* (*35*) showed that more than 10 or even dozens of parallel specimens may be needed to achieve a reasonable level of confidence in typical small-scale laboratory experiments. However, the number of replicate specimens is usually lower, typically ranging from 1 to 5. This may explain, at least partly, the huge scatter in literature data (*11*) for C_{crit}.

Another implication of our findings (Fig. 1) is that results from small-scale laboratory tests are not directly applicable to engineering structures. Several researchers have reported relatively high C_{crit} from laboratory experiments compared to practical experience (*27*, *37*, *45*–*47*). This discrepancy is generally ascribed to superior material properties of laboratory specimens compared to the conditions achieved on construction sites, particularly regarding macroscopic concrete voids at the SCI or inhomogeneities in steel surface conditions (*46*). We suggest consideration of size effects as an alternative explanation for higher laboratory C_{crit} compared to engineering structures—that is, consideration of the fact that laboratory specimens are generally of small dimensions and that this factor, given a specific type of concrete and type of steel, increases C_{crit}. This possibility is underscored by the present observation that coarse voids, which may generally be more frequently found in site-produced concretes than in laboratory specimens, appear not to have an adverse effect on C_{crit}, at least not under wetting/drying exposure conditions.

Another implication of the size effect concerns common techniques and sensors used for monitoring corrosion in engineering structures. Typically, these approaches are based on carbon steel specimens embedded at increasing depths in the concrete cover (*48*–*51*). These serve as corrosion detection probes, that is, they are monitored until corrosion initiates at a probe at a certain depth. From this, the time to corrosion

of the structural reinforcing steel, being located at a greater depth, is extrapolated. The surface area of the corrosion detection probes may range from a fraction of 1 cm^2 up to ~50 cm^2 (*48*–*53*). Thus, these sensors typically have an exposed surface area somewhere between series S and M in this work. In the light of the results presented here, these relatively small sensors are expected to require higher chloride concentrations to start corroding than the reinforcing steel in the same structure. If this fact is ignored, predictions based on the sensor may lead to an overestimation of the time to corrosion of the reinforcing steel. This may be counteracted by increasing the number of sensors at a given depth and by applying the weakest link theory for the needed transformation regarding size (Eq. 1). However, another possible limitation of some of these sensor systems is that the steel type and surface are not representative of the structural reinforcing steel.

Finally, an important implication of our findings regards the concept of C_{crit}, which is a concept describing a limit state for corrosion. For this concept to be successfully applied in service life predictions of engineering structures, it is crucial to incorporate the size effect. In the current state of the art, this is not the case; over the past >60 years, chloride threshold values in concrete have typically been characterized on laboratory specimens of relatively small dimensions. However, if the dimensions of the specimens from which the results are obtained are ignored in service life modeling, the predicted time to corrosion initiation may be considerably underestimated or overestimated.

A number of authors have shown that service life models are strongly sensitive to C_{crit}, that is, that even small uncertainties in C_{crit} give rise to large uncertainties in terms of the predicted time to corrosion (*5*, *54*, *55*). This may be illustrated by means of a simple prediction of chloride ingress into concrete, as described by Tang *et al.* (*8*, *56*), and by calculating the time to corrosion as the time until the predicted chloride concentration in the concrete equals C_{crit}. The example displayed in fig. S3 shows this for an assumed cover depth of 50 mm and using the different C_{crit} according to Fig. 1 as input parameters. In this case, the average time to corrosion is ~40 years in the 100-cm-long specimens (L) and ~110 years in the 10-cm-long specimens (M). Thus, an increase in C_{crit} by ~50% (from μ = 0.80% chloride by weight of cement for L to μ = 1.25% chloride by weight of cement for M) corresponds to an increase in predicted time to corrosion by a factor of almost 3 (from 40 years for L to 110 years for M). This amplifying effect is due to the fact that the increase in chloride concentration at a given cover depth slows down with time, that is, that after a few decades in the life of a structure, considerably more time is needed for even a slight increase in chloride concentration. In the 1-cm-long specimens (S), the predicted minimum time to corrosion even exceeds 1000 years. In summary, by influencing C_{crit}, the size effect of corrosion of steel in concrete greatly influences the predicted life span of concrete structures.

To make the needed leap forward in forecasting reinforcing steel corrosion in concrete, further research studies should address the following issues: (i) quantifying the size effect on real systems (that is, testing reinforcing steel bars exhibiting surface conditions representative for construction sites and embedded in mature site-produced concrete). A limitation of laboratory studies, including the present one, is that corrosion is investigated under conditions that may not be representative of engineering structures. Because variability in a number of local properties of the SCI is expected to be more pronounced in engineering structures compared to laboratory specimens (*13*), the size effect may also tend to be more significant in these structures. We consider it important to experimentally validate this and to quantify the size effect for practical conditions. (ii) To permit taking the size effect into account in service life predictions of concrete structures, there is a need to combine materials science and structural engineering (mechanical behavior). Probabilistic service life models require the statistical distribution of C_{crit} as input parameter. Because this depends on size (Fig. 1), engineers need to be able to identify the reinforcing steel bar length (size) that is relevant in different reinforced concrete members in engineering structures on the basis of mechanical considerations (*35*). (iii) Finally, there are still many open questions concerning the role of the SCI in corrosion initiation. To enhance predictive models for corrosion in concrete, it is essential to deliver a better understanding of the relative importance of the different local features of the SCI in controlling initiation (or inhibition) of corrosion of steel in concrete.

MATERIALS AND METHODS

Experimental design

This study aimed at testing the hypothesis of a size-scale effect of chloride-induced steel corrosion in concrete. Reinforced concrete beams of different lengths were manufactured, and their susceptibility to corrosion was studied. Subsequent analyses aimed at revealing correlations between the sites where localized corrosion initiated and the local conditions at the SCI.

Specimen preparation

Reinforced concrete specimens were manufactured in the laboratory with concrete made from Portland cement and a water/cement ratio of 0.5. The detailed concrete mix proportions are given in table S2. The reinforcing steel bars [class B500B according to (*57*), cold-work strengthened] had a diameter of 10 mm. When delivered, they were free of any surface rust. Before casting, the surface was degreased with acetone but otherwise left in as-received condition.

Figure S4 details the geometry of the molds used for casting the specimens; the steel bars were oriented vertically during casting. After casting, the specimens were left for self-desiccation for 28 days and were then cut, as shown in fig. S5. The final reinforced concrete beams had a cross section of 7-cm width and 9-cm height; the length was variable. After cutting, a cable connection was established to each steel bar (screw connection). All specimens were painted with an epoxy coating to achieve a defined exposed length L_{exp} (Fig. 1A and fig. S5). Three different L_{exp} were studied in this work, namely 1, 10, and 100 cm; the series were termed S, M, and L, respectively. The numbers of replicate specimens were six for series L and eight each for series M and S (Fig. 1). The steel bar ends were either protected by a duplex shielding similar to the studies of Angst *et al.* (*27*) and Lambert *et al.* (*46*) or by avoiding access to chloride with help of the epoxy coating on the exposed surface (more detailed information given in figs. S5 and S6); visual inspection of the steel bars after terminating the experiments confirmed that this approach was suitable to avoid corrosion at the bar ends.

Corrosion tests

After 4 months of exposure to indoor climate [that is, with the uncoated surfaces exposed to approximately 50 to 60% relative humidity (RH) (temperature, 20° ± 2°C)], the specimens were placed with the cut surfaces facing downward in demineralized water. The depth of immersion was only 1 cm (that is, the upper concrete surface was exposed to air). Over time, the chloride concentration in the solution was increased step-wise by adding sodium chloride. At certain times, the specimens

were lifted and exposed to air (approximately 50 to 60% RH). The detailed wetting/drying cycles are given in table S3.

For the entire corrosion test, the upper and the lower steel bar in each specimen were electrically connected. During the wetting cycles, the steel potential was measured with help of a reference electrode (saturated silver/silver chloride electrode) immersed in the solution. All measurements were carried out with an automated data logger (input impedance > 10^{10} ohms); the measurement interval was 1 hour. Corrosion initiation was detected by a pronounced drop in potential. On the basis of the studies of Angst *et al.* (*27*, *28*, *58*), the criterion for initiation of stable corrosion was as follows: a potential drop by at least 120 mV within a short time (1 to 2 days), after which the negative level of potential is maintained over at least 5 days.

Sampling procedures and examination

After stable corrosion initiation was detected, the corresponding specimen was withdrawn from the exposure test and destructively examined. This happened within a maximum of 10 days after corrosion initiation. Mechanically splitting the specimen permitted the removal of the steel bar from the concrete. Both the steel bar and the imprint left in the concrete were visually inspected to identify the location of corrosion initiation and to correlate it with visually apparent characteristics at the SCI. After a first inspection of the steel bar, the steel surface was cleaned from adhering concrete phases and from deposited corrosion products by immersion in an inhibited pickling solution [hydrochloric acid (1:1) + 3 g/liter of urotropine (hexamethylenetetramine)] in an ultrasonic bath for 1 to 2 min.

At the cover depth, a 3- to 4-mm-thick disc of concrete was cut (that is, at the cover depth of ±1.5 to 2.0 mm), with lateral dimensions of approximately 3 cm × 10 cm. This concrete sample was dried to constant weight at 105°C and subsequently milled, from which >20-g concrete powder was obtained. The content of acid-soluble chlorides was determined in the concrete powder samples according to standard (*59*) and considered as C_{crit} for the actual specimen.

In addition to sampling at the location of corrosion initiation, sections perpendicular to the steel bar were cut from selected concrete beams before splitting to examine the SCI. This was performed with specimens of series S (which did not initiate corrosion) and of series L (in zones far from where corrosion started). For the latter, the corroding zone could be reliably located by moving a reference electrode along the concrete surface. The cut sections were dried in air, impregnated with epoxy resin under vacuum, and finally grounded and polished to a flat surface before studied under scanning electron microscopy (SEM).

Finally, on the basis of visual inspection of the removed reinforcing steel bars, sections perpendicular to the steel bar were cut at the locations of corrosion initiation. These metallurgical sections were polished (silicon carbide papers of up to 1200 grit; 6-µm and 3-µm diamond spray; and finally, 0.05-µm Al_2O_3 suspension), etched (3% Nital, for approximately 10 s), and then examined with light optical microscopy.

Probabilistic modeling

Log-normal probability distributions were fitted to the experimentally obtained C_{crit} for series M and L. The fitting parameters were

$$\lambda = E(\ln(C_{crit})) \quad (2)$$

$$\varepsilon^2 = \mathrm{var}(\ln(C_{crit})) \quad (3)$$

The first two moments ("as measured" rather than log-normally transformed) are (*34*, *35*)

$$\mu = E(C_{crit}) = \exp\left(\lambda + \frac{1}{2}\varepsilon^2\right) \quad (4)$$

$$\sigma^2 = \mathrm{var}(C_{crit}) = \mu^2 \cdot (\exp(\varepsilon^2) - 1) \quad (5)$$

On the basis of these parameters for series M, the probability distribution of C_{crit} could be predicted for larger L_{exp}, following the procedure described by Angst *et al.* (*35*). This consists of calculating the probability for corrosion, p_L, for discrete chloride contents, according to Eq. 1, and by using the log-normal distribution obtained for series M as p_M.

SUPPLEMENTARY MATERIALS

Supplementary material for this article is available at http://advances.sciencemag.org/cgi/content/full/3/8/e1700751/DC1

fig. S1. Examples of coarse air voids at the SCI.
fig. S2. Morphology of the corrosion attack.
fig. S3. Example of prediction of time to corrosion initiation.
fig. S4. Reinforced concrete slabs cast in the laboratory.
fig. S5. Preparation of specimens of different sizes based on the slabs shown in fig. S4.
fig. S6. Detail of end-shielding of the steel bars.
table S1. Detailed results of measured chloride threshold values C_{crit} for corrosion initiation.
table S2. Nominal concrete mix proportions.
table S3. Wetting/drying exposure and sampling times after corrosion initiation for the individual specimens.

REFERENCES AND NOTES

1. C. L. Page, Mechanism of corrosion protection in reinforced concrete marine structures. *Nature* **258**, 514–515 (1975).
2. British Cement Association, "Development of an holistic approach to ensure the durability of new concrete construction" (Research Report Project 38/13/21 (cc 1031), British Cement Association, 1997).
3. G. H. Koch, M. P. H. Brongers, N. G. Thompson, Y. P. Virmani, J. H. Payer, Corrosion costs and preventive strategies in the United States. *Mater. Perf.* **42**, 1–12 (2002).
4. L. Bertolini, B. Elsener, P. Pedeferri, E. Redaelli, R. Polder, *Corrosion of Steel in Concrete: Prevention, Diagnosis, Repair* (Wiley-VCH, ed.2, 2013).
5. C. L. Page, M. M. Page, *Durability of Concrete and Cement Composites* (Woodhead Publishing Ltd., 2007), 404 pp.
6. R. B. Polder, W. H. A. Peelen, W. M. G. Courage, Non-traditional assessment and maintenance methods for aging concrete structures—Technical and non-technical issues. *Mater. Corros.* **63**, 1147–1153 (2012).
7. M. Raupach, doctoral thesis, Aachen University, Germany (1992).
8. L. Tang, L.-O. Nilsson, M. P. A. Basheer, *Resistance of Concrete to Chloride Ingress: Testing and Modelling* (CRC Press, 2012).
9. W. Breit, Critical corrosion inducing chloride content – State of the art and new investigation results, in *Betontechnische Berichte 1998-2000* (Verein Deutscher Zementwerke e.V., 2001).
10. M. C. Alonso, M. Sanchez, Analysis of the variability of chloride threshold values in the literature. *Mater. Corros.* **60**, 631–637 (2009).
11. U. Angst, B. Elsener, C. K. Larsen, Ø. Vennesland, Critical chloride content in reinforced concrete—A review. *Cem. Concr. Res.* **39**, 1122–1138 (2009).
12. C. L. Page, Initiation of chloride-induced corrosion of steel in concrete: Role of the interfacial zone. *Mater. Corros.* **60**, 586–592 (2009).
13. U. M. Angst, M. R. Geiker, A. Michel, C. Gehlen, H. Wong, O. B. Isgor, B. Elsener, C. M. Hansson, R. François, K. Hornbostel, R. Polder, M. C. Alonso, M. Sanchez, M. J. Correia, M. Criado, A. Sagüés, N. Buenfeld, The steel–concrete interface. *Mater. Struct.* **50**, 143 (2017).
14. R. C. Mielenz, V. E. Wolkodoff, J. E. Backstrom, H. L. Flack, Orgin, evolution, and effects of the air void system in concrete. Part 1—entrained air in unhardened concrete. *Proc. Am. Concr. Inst.* **55**, 95–121 (1958).
15. R. C. Mielenz, V. E. Wolkodoff, J. E. Backstrom, R. W. Burrows, Orgin, evolution, and effects of the air void system in concrete part 4—The air void system in job concrete. *Proc. Am. Concr. Inst.* **55**, 507–517 (1958).

16. G. T. Burstein, P. C. Pistorius, S. P. Mattin, The nucleation and growth of corrosion pits on stainless steel. *Corros. Sci.* **35**, 57–62 (1993).
17. G. Wranglen, Pitting and sulphide inclusions in steel. *Corros. Sci.* **14**, 331–349 (1974).
18. G. T. Burstein, G. O. Ilevbare, The effect of specimen size on the measured pitting potential of stainless steel. *Corros. Sci.* **38**, 2257–2265 (1996).
19. L. Li, A. A. Sagües, Chloride corrosion threshold of reinforcing steel in alkaline solutions—Effect of specimen size. *Corrosion* **60**, 195–202 (2004).
20. U. R. Evans, *The Corrosion and Oxidation of Metals: Scientific Principles and Practical Applications* (Edward Arnold Ltd., 1960), pp. 911–950.
21. N. R. Buenfeld, G. K. Glass, B. Reddy, R. F. Viles, Process for the protection of reinforcement in reinforced concrete, U.S. Patent 6,685,822 B2 (2004).
22. T. A. Soylev, R. François, Quality of steel–concrete interface and corrosion of reinforcing steel. *Cem. Concr. Res.* **33**, 1407–1415 (2003).
23. A. Castel, T. Vidal, R. François, G. Arliguie, Influence of steel–concrete interface quality on reinforcement corrosion induced by chlorides. *Mag. Concr. Res.* **55**, 151–159 (2003).
24. P. Ghods, O. B. Isgor, G. A. McRae, J. Li, G. P. Gu, Microscopic investigation of mill scale and its proposed effect on the variability of chloride-induced depassivation of carbon steel rebar. *Corros. Sci.* **53**, 946–954 (2011).
25. G. Fagerlund, "Moisture design with regards to durability – with special reference to frost destruction" (Report TVBM-3130, Lund University, 2006).
26. G. Fagerlund, "The long time water absorption in the air-pore structure of concrete" (Report TVBM-3051, Lund University, 1993).
27. U. M. Angst, B. Elsener, C. K. Larsen, Ø. Vennesland, Chloride induced reinforcement corrosion: Electrochemical monitoring of initiation stage and chloride threshold values. *Corros. Sci.* **53**, 1451–1464 (2011).
28. U. Angst, M. Wagner, B. Elsener, A. Leemann, P. V. Nygaard, "Method to determine the critical chloride content of existing reinforced concrete structures" (Research Report no. 677, AGB 2012/010 (in German), Swiss Federal Roads Office, 2016).
29. A. T. Horne, I. G. Richardson, R. M. D. Brydson, Quantitative analysis of the microstructure of interfaces in steel reinforced concrete. *Cem. Concr. Res.* **37**, 1613–1623 (2007).
30. A. Delagrave, J. P. Bigas, J. P. Ollivier, J. Marchand, M. Pigeon, Influence of the interfacial zone on the chloride diffusivity of mortars. *Adv. Cem. Based Mater.* **5**, 86–92 (1997).
31. P. Goltermann, Variation of chloride profiles in homogeneous areas. *Mater. Struct.* **37**, 608–614 (2004).
32. A. Soive, V. Baroghel-Bouny, Influence of gravel distribution on the variability of chloride penetration front in saturated uncracked concrete. *Constr. Build. Mater.* **34**, 63–69 (2012).
33. U. M. Angst, R. Polder, Spatial variability of chloride in concrete within homogeneously exposed areas. *Cem. Concr. Res.* **56**, 40–51 (2014).
34. R. E. Melchers, *Structural Reliability Analysis and Prediction* (John Wiley & Sons, ed. 2, 1999).
35. U. Angst, A. Rønnquist, B. Elsener, C. K. Larsen, Ø. Vennesland, Probabilistic considerations on the effect of specimen size on the critical chloride content in reinforced concrete. *Corros. Sci.* **53**, 177–187 (2011).
36. C. M. Hansson, B. Sørensen, The threshold value of chloride concentration for the corrosion of reinforcement in concrete, in *Corrosion Rates of Steel in Concrete*, N. S. Berke, V. Chaker, D. Whiting, Eds. (ASTM, 1989), pp. 3–16.
37. K. Pettersson, "Corrosion threshold value and corrosion rate in reinforced concrete" (CBI report 2:92, Swedish Cement and Concrete Research Institute, 1992).
38. P. Sandberg, "Chloride initiated reinforcement corrosion in marine concrete" (Report TVBM-1015, Lund University, 1998).
39. B. H. Oh, S. Y. Jang, Y. S. Shin, Experimental investigation of the threshold chloride concentration for corrosion initiation in reinforced concrete structures. *Mag. Concr. Res.* **55**, 117–124 (2003).
40. O. Poupard, A. Aït-Mokhtar, P. Dumargue, Corrosion by chlorides in reinforced concrete: Determination of chloride concentration threshold by impedance spectroscopy. *Cem. Concr. Res.* **34**, 991–1000 (2004).
41. A. M. Neville, *Properties of Concrete* (Pearson Education Limited, ed. 5, 2011).
42. V. K. Gouda, W. Y. Halaka, Corrosion and corrosion inhibition of reinforcing steel: II. Embedded in concrete. *Br. Corros. J.* **5**, 204–208 (1970).
43. M. Thomas, Chloride thresholds in marine concrete. *Cem. Concr. Res.* **26**, 513–519 (1996).
44. P. Schiessl, W. Breit, Local repair measures at concrete structures damaged by reinforcement corrosion, in *Proceedings of the Fourth International Symposium Corrosion of Reinforcement in Concrete Construction*, C. L. Page, P. Bamforth, J. W. Figg, Eds. (The Royal Society of Chemistry, 1996), pp. 525–534.
45. C. Alonso, M. Castellote, C. Andrade, Chloride threshold dependence of pitting potential of reinforcements. *Electrochim. Acta* **47**, 3469–3481 (2002).
46. P. Lambert, C. L. Page, P. R. W. Vassie, Investigations of reinforcement corrosion. 2. Electrochemical monitoring of steel in chloride-contaminated concrete. *Mater. Struct.* **24**, 351–358 (1991).
47. M. Manera, Ø. Vennesland, L. Bertolini, Chloride threshold for rebar corrosion in concrete with addition of silica fume. *Corros. Sci.* **50**, 554–560 (2008).
48. O. E. Gjørv, Ø. Vennesland, A new probe for monitoring steel corrosion in offshore concrete platforms. *Mater. Perform.* **21**, 33–35 (1982).
49. P. Schiessl, M. Raupach, Monitoring system for the corrosion risk of steel in concrete structures. *Concr. Int.* **14**, 52–55 (1992).
50. P. Schiessl, Neue Sensortechnik zur Überwachung von Bauwerken. *Int. Zeitschr. f. Bauinstandsetzen* **2**, 189–209 (1996).
51. M. Raupach, P. Schiessl, Monitoring system for the penetration of chlorides, carbonation and the corrosion risk for the reinforcement. *Constr. Build. Mater.* **11**, 207–214 (1997).
52. H. S. Lee, S. W. Shin, J. M. Ahn, Y. C. Kim, Y. T. Kho, Development of corrosion sensors for monitoring steel-corroding agents in reinforced concrete structures. *Mater. Corros.* **54**, 229–234 (2003).
53. K. R. Larsen, Evaluating sensors to monitor steel corrosion in concrete structures. *Mater. Perf.* **54**, 17–19 (2015).
54. U. M. Angst, B. Elsener, Chloride threshold values in concrete—A look back and ahead, in "Chloride limits and thresholds for concrete containing supplementary cementitious materials (SCMs)" (SP-308, American Concrete Institute, 2016), pp. 1–12.
55. J. Gulikers, Considerations on the reliability of service life predictions using a probabilistic approach. *J. Phys.* **136**, 233–241 (2006).
56. *Model Code for Service Life Design* (fib bulletin no. 34, International Federation for Structural Concrete, 2006).
57. European Committee for Standardization, *BS EN 10080:2005—Steel for the Reinforcement of Concrete. Weldable Reinforcing Steel. General* (2005).
58. RILEM Technical Committee 235-CTC, "Corrosion initiating chloride threshold concentrations in concrete" (2009–2015); www.rilem.org/gene/main.php?base=8750&gp_id=237.
59. Schweizerischer Ingenieur- und Architektenverein SIA, *SN EN 14629:2007: Products and Systems for the Protection and Repair of Concrete Structures—Test Methods—Determination of Chloride Content in Hardened Concrete* (2008).

Acknowledgments: We thank G. Peschke, A. M. A. Sanchez, C. Boschmann, and H. Richner for their technical assistance. We also thank R. J. Flatt for his useful comments. **Funding:** No funding was received for this work. **Author contributions:** U.M.A. conceived, designed, and performed the experiments. All authors contributed to the interpretation of the data and writing the manuscript. **Competing interests:** The authors declare that they have no competing interests. **Data and materials availability:** All data needed to evaluate the conclusions in the paper are present in the paper and/or the Supplementary Materials. Additional data related to this paper may be requested from the authors.

Submitted 13 March 2017
Accepted 28 June 2017
Published 2 August 2017
10.1126/sciadv.1700751

Citation: U. M. Angst, B. Elsener, The size effect in corrosion greatly influences the predicted life span of concrete infrastructures. *Sci. Adv.* **3**, e1700751 (2017).